Constraining the Intermodel Spread in Cloud and Water Vapor Feedback

Haozhe He[1], Ryan J Kramer[2], and Brian Soden[3]

[1]University of Miami
[2]NASA/USRA
[3]Univ. Miami, Miami

November 23, 2022

Abstract

Uncertainty in climate feedbacks is the primary source of spread in model projections of surface temperature response to anthropogenic forcing. Cloud feedback persistently appears as the main source of disagreement in future projections while the combined lapse-rate plus water vapor (LR+WV) feedback is a smaller (~30%), but non-trivial source of uncertainty in climate sensitivity. Here observation-based emergent constraints are adopted to evaluate the intermodel spread in these feedbacks. The observed interannual variation provides a useful constraint on the long-term cloud feedback as evidenced by the consistency between their global-mean values as well as their similar regional contributions to the intermodel spread. However, internal variability does not serve to constrain the long-term LR+WV feedback spread, which we find is mostly associated with the relative humidity response over the tropics. Model differences in hemispheric warming asymmetries, induced primarily by ocean heat uptake differences, also contribute to the spread in water vapor feedback.

Constraining the Intermodel Spread in Cloud and Water Vapor Feedback

Haozhe He[1], Ryan J. Kramer[2,3], Brian J. Soden[1]

[1]Rosenstiel School of Marine and Atmospheric Science, University of Miami, Miami, FL, USA

[2]Climate and Radiation Laboratory, NASA Goddard Space Flight Center, Greenbelt, MD, USA

[3]Universities Space Research Association, Columbia, MD, USA

Correspondence to: Haozhe He, haozhe.he@rsmas.miami.edu

Submitted to Geophysical Research Letters

Abstract

Uncertainty in climate feedbacks is the primary source of spread in model projections of surface temperature response to anthropogenic forcing. Cloud feedback persistently appears as the main source of disagreement in future projections while the combined lapse-rate plus water vapor (LR+WV) feedback is a smaller (~30%), but non-trivial source of uncertainty in climate sensitivity. Here observation-based emergent constraints are adopted to evaluate the intermodel spread in these feedbacks. The observed interannual variation provides a useful constraint on the long-term cloud feedback as evidenced by the consistency between their global-mean values as well as their similar regional contributions to the intermodel spread. However, internal variability does not serve to constrain the long-term LR+WV feedback spread, which we find is mostly associated with the relative humidity response over the tropics. Model differences in hemispheric warming asymmetries, induced primarily by ocean heat uptake differences, also contribute to the spread in water vapor feedback.

Key Points:

Observed interannual variation provides a useful constraint to narrow the uncertainty in long-term cloud feedback.

It is difficult to constrain the long-term LR+WV feedback uncertainty with available observations of interannual variability.

Disagreements in the responses of tropical relative humidity and ocean heat uptake are responsible for the spread in long-term LR+WV feedback.

Plain Language Summary

How much the Earth warms in response to greenhouse gas increases depends on the Earth's efficiency in restoring radiative equilibrium. This efficiency differs significantly among global climate models due to differences in feedback processes, particularly the responses of clouds, temperature and water vapor to the initial perturbation. One approach to narrowing the intermodel spread of feedbacks is to only consider models whose observable variability is consistent with available measurements. For example, the similar behavior of both interannual and long-term cloud feedbacks enables observations to effectively constrain cloud feedback. However, this approach does not work for the feedback resulting from changes in the vertical distribution of temperature and water vapor (LR+WV feedback). The global-mean LR+WV feedback uncertainty mostly comes from the tropics, where local relative humidity exhibits the largest intermodel disagreement. Model differences in meridional warming imbalance, stemming from divergent ocean energy absorptions, also account for the global-mean LR+WV feedback uncertainty.

1. Introduction

The projected surface air temperature responses to anthropogenic forcing have a large spread among global climate models, primarily due to large uncertainties in climate feedbacks (Flato et al., 2013). Particularly, cloud feedback has persistently been identified as the largest source of intermodel spread in effective climate sensitivity (ECS; Dufresne & Bony, 2008; Vial et al., 2013; Zelinka et al., 2020). Although the cloud feedback appears positive in most models and thereby acts to amplify global warming, its magnitude differs substantially among models (Colman, 2003; Soden & Held, 2006; Soden et al., 2008; Zelinka et al., 2020). Accurately simulating clouds and their radiative responses has long been a stubborn challenge for climate modeling, largely because clouds depend on fine-scale physical processes that cannot be explicitly represented by coarse model grids. Although the representations of cloud processes have been improved in state-of-the-art climate models, such as more accurate representation of supercooled liquid cloud water, the range of global-mean cloud feedback in the most recent generation of models has actually increased slightly (Bjordal et al., 2020; Zelinka et al., 2020).

Another important component in understanding the uncertainty of ECS is temperature feedback induced by tropospheric warming, which includes contributions from a vertically uniform warming (Planck feedback) and departures from the vertical-uniform warming [lapse-rate (LR) feedback]. The latter constituent further leads to a large spread in water vapor (WV) feedback, since atmospheric moistening to first order follows the Clausius-Clapeyron relation. As these two components are so tightly coupled in models, it is physically logical to analyze the combined lapse-rate plus water vapor (LR+WV) feedback, instead of each term individually (Held & Soden, 2000). Even though there is cancellation between LR and WV feedbacks in both magnitude and uncertainty, LR+WV feedback still possesses the second largest contribution to the intermodel spread of ECS (Dufresne & Bony 2008; Vial et al. 2013). Soden and Held (2006) noted that, individually, the global-mean LR and WV feedbacks are strongly related to the ratio of tropical to global-mean surface warming. However, the global-mean LR+WV feedback is largely driven by local model differences over the southern extratropics (Po-Chedley et al., 2018), highlighting the role of Southern Ocean heat uptake in determining the global-mean LR+WV feedback.

Here we reexamine the sources of intermodel spread in cloud and LR+WV feedback, using conventional local feedback definition with global-mean surface air temperature anomalies. This allows us to clearly isolate contributions from uncertainties in local radiative responses and surface warming patterns, respectively. Compared to Po-Chedley et al. (2018), we find the global-mean LR+WV feedback uncertainty mostly comes from the tropics, where local relative humidity exhibits the largest intermodel disagreement, instead of the southern extratropics. We also find a weaker correlation between LR+WV and relative humidity fixed LR feedbacks than Po-Chedley et al. (2018). Additionally, we extend the well-established emergent constraint method (e.g., Klein & Hall, 2015) to these long-standing climate feedback challenges, to investigate its utility in narrowing the spread of these feedbacks, thereby refining the estimate of ECS.

2. Data and Methodology

Climate feedbacks represent the amplification or dampening of radiative flux anomalies to internal variabilities or externally forced changes in global-mean surface air temperature. Using observationally based radiative kernels derived from CloudSat/CALIPSO data (Kramer et al., 2019), we decompose top-of-atmosphere radiative flux anomalies into radiation changes caused by variations in temperature, water vapor, albedo and cloud, following Soden et al. (2008). Here, cloud radiative response is diagnosed from change in cloud radiative effect corrected for cloud masking effects on non-cloud radiative responses. Note that the cloud radiative response is the sum of its longwave and shortwave components. Based on documented relationships between longwave and shortwave components for different cloud types (Webb et al., 2006), we further separate the cloud radiative responses into contributions from high, low and mixed clouds, following Soden and Vecchi (2011). The LR+WV radiative response is the sum of LR and WV radiative responses. Since differences in cloud climatologies can influence analyses of all-sky LR+WV feedback, we focus primarily on uncertainties in clear-sky LR+WV feedback in the main text, while further details of all-sky LR+WV feedback are provided in the supplemental material.

Climate models (Table S1) from Coupled Model Intercomparison Project Phase 6 (CMIP6; Eyring et al., 2016), with r1i1p1f1 realization available for both piControl and abrupt-4xCO2 experiments, are evaluated in this work. Following Dessler (2013), interannual climate feedbacks are calculated as the linear regression slope of monthly deseasonalized global-mean radiative flux anomalies against monthly deseasonalized global-mean surface air temperature anomalies, using CMIP6 pre-industrial control (piControl) runs. To obtain the interannual climate feedbacks as accurately as possible, the longest simulation length available for all models (200 years) is used. In the piControl runs, variations of global-mean surface air temperature are induced solely by internal variability in the climate system, which is primarily caused by El Niño–Southern Oscillation, especially on interannual timescales. No climate drift is noted in the time series of cloud or LR+WV radiative responses. Climate feedbacks in response to long-term climate change are calculated as the linear regression slope of annual global-mean radiative flux anomalies against annual global-mean surface air temperature anomalies from 150-year experiments, where CO_2 concentrations are abruptly quadrupled at the beginning and then held constant as the climate system responds (abrupt-4xCO2). Although the time-invariant feedback assumption adopted here is undermined by evolving pattern effects (e.g., Andrews et al., 2015; Chung & Soden, 2015; Andrews & Webb, 2018; Dong et al. 2020), the assumption is still useful for investigating the intermodel spread, since no noticeable difference occurs between the spreads of feedbacks derived from regressions over years 1–150 and years 21–150 of abrupt-4xCO2 simulations (e.g., Zhou et al., 2015).

To evaluate the model-simulated global-mean feedbacks, observation-based interannual emergent constraints are adopted. The observed interannual feedbacks are calculated using radiative fluxes from CERES Energy Balance and Filled (EBAF) Ed. 4.1 product (Loeb et al., 2018, 2019), vertical profiles of temperature and water vapor from ERA5 (Hersbach, 2020) and surface temperature from GISS Surface Temperature Analysis (GISTEMP v4; Lenssen, 2019; GISTEMP Team, 2020). The corresponding 95% confidence intervals are calculated using uncertainties (i.e., standard deviation) of the observed interannual feedbacks (i.e., linear regression slope) to provide observed uncertainty bounds. In addition, vertical profiles from version 6 Level 3 AIRS retrievals (Aumann, 2003) and Modern-Era Retrospective Analysis for Research and Applications, Version 2 (MERRA-2; Gelaro, 2017) reanalysis are adopted for potential cross-validations. Because of the limited length of satellite observations, the observation-based estimates without (with) AIRS retrievals are conducted over the period of 2001 (2003) through 2019.

3. Results

3.1 Emergent constraints

The emergent constraint method has been applied to help reduce the persistent intermodel spread of climate feedbacks (e.g., Hall & Qu, 2006; Qu & Hall, 2014). One key principle of the emergent constraint idea is that models failing to reproduce observed characteristics in unforced or historical simulations should not be trusted for future climate projection, especially if that characteristic in question is physically and statistically related on these timescales (Klein & Hall, 2015). Here, comparisons between global-mean interannual and long-term feedbacks are conducted. As shown in Figure 1a, there is a strong correlation (r = 0.84) between interannual and long-term cloud feedbacks. With a least-squares regression slope of 0.81, the intermodel spread of cloud feedback is comparable on these timescales, which differs from previous findings using CMIP5-era models (Zhou et al., 2015; Colman & Hanson, 2017). For instance, Zhou et al. (2015) found the model-averaged global-mean long-term cloud feedback is smaller than its interannual counterpart. This results, in part, from a slight increase in long-term cloud feedback (Zelinka et al., 2020) and a decrease in global-mean interannual cloud feedback in CMIP6-era models.

Since the global-mean long-term and interannual cloud feedbacks are closely related in both magnitude and uncertainty, it is possible to observationally constrain the former by identifying models with interannual cloud feedbacks that fall within the observed uncertainty (i.e., 95% confidence interval). In this case, the lower tier of models is inconsistent with observed uncertainty estimates. If one excludes those models, the intermodel spread of long-term cloud feedback could be narrowed by approximately one-third. Since the ECS of a model is tied to the strength of its cloud feedback (e.g., Zelinka et al., 2020), our findings suggest a low ECS is unlikely, consistent with conclusions by Sherwood et al. (2020).

Figure 1b compares interannual and long-term LR+WV feedbacks. Although the correlation between global-mean interannual and long-term LR+WV feedbacks is statistically significant at the 99% level, virtually all models fall within the observed uncertainty. This is due to two reasons. First, the spread of long-term LR+WV feedback (1.32 ~ 1.67 W m^{-2} K^{-1}) is only half of that of interannual feedback (1.07 ~ 1.73 W m^{-2} K^{-1}). Second, the observational-interannual uncertainty is nearly equal to the intermodel spread. Additionally, the observed interannual LR+WV feedbacks differ considerably among different observational and reanalyses products, reflecting the large degree of uncertainty in available observations of temperature and humidity profiles (Kramer et al., 2021). Similar results are seen in all-sky LR+WV feedback (Figure S1a), with an even weaker correlation between global-mean interannual and long-term LR+WV feedback.

Surprisingly, the spread of tropical-mean long-term LR+WV feedback (1.61 ~ 2.37 W m^{-2} K^{-1}) is twice as large as the global-mean spread. This is counter-intuitive. Since tropical atmosphere has long been known for following well-documented processes (i.e., moist adiabatic lapse-rate and radiative-convective equilibrium; e.g., Santer et al., 2005), one might expect the spread of tropical-mean LR+WV feedback to be smaller than the global-mean spread. This motivates us to further explore the sources of intermodel spread in these feedbacks.

3.2 Intermodel spread analyses

To quantify local contribution of feedbacks to the global-mean intermodel spread, a simple linear regression method is adopted:

$$FB_{local} = aFB_{global} + b$$

Here, FB_{local} is the intermodel variation of local feedbacks, which is resolved at each grid point. The interannual (long-term) FB_{local} from each model is calculated in traditional way, by regressing deseasonalized (annual) local radiative response against deseasonalized (annual) global-mean surface air temperature anomalies, instead of local surface air temperature anomalies. In this way, we isolate indirect effects of local surface temperature change exerted on local radiative responses. FB_{global} is the intermodel variation of global-mean feedbacks, which is the same for each grid. The “a” is the contribution from local intermodel uncertainty to the global-mean feedback spread. When FB_{local} spread is large and varies with FB_{global}, we can obtain a large value of “a”, suggesting a large contribution from local difference to the global-mean spread.

The spatial distribution of this contribution will be referred to as "contribution pattern" hereafter. The "b" is the y-intercept of the linear regression, a meaningless parameter in this method.

Figures 2a-b highlight the contribution from local cloud feedback differences to the spread in global-mean cloud feedback. The contribution patterns for interannual and long-term cloud feedbacks exhibit similar characteristics. Specifically, local feedback differences over the eastern Pacific and Southern Ocean contribute the most to the global-mean cloud feedback spread on both timescales. Additionally, most of regions with statistically significant contribution to the global-mean cloud feedback spread are associated with low clouds. This supports the utility of the observed constraint on global-mean long-term cloud feedback, since an emergent constraint must be based on a coherent relationship between intermodel variations in an observable quantity and in its future projection (Klein & Hall, 2015). This consistency between interannual and long-term contribution patterns is also evident in both shortwave and longwave cloud feedbacks (Figure 2c-f), although the magnitude of local contribution on long-term timescales is generally smaller than that on interannual timescales. As expected, the shortwave component dominates local contributions to global-mean, total cloud feedback (Figure 2a-d & S2a-d), given the considerable importance of low cloud feedback.

A similar analysis is applied to the LR+WV feedback (Figure 3a-b & S3a-b). Generally, the spread of global-mean LR+WV feedback is driven by feedbacks over the tropics on both interannual and long-term timescales. However, the contribution patterns are noticeably different on these timescales. For instance, the intermodel spread of long-term LR+WV feedback is driven by a hemispheric asymmetric contribution pattern which is not observed on interannual timescales. This difference highlights the challenge in using observed variability to constrain global-mean long-term LR+WV feedback, since it points to differences in these feedbacks on a physical level.

Interestingly, the spread in global-mean long-term LR+WV feedback is partly reduced due to compensation between the northern and southern hemispheres (NH & SH). Models with an anomalously strong NH feedback tend to have an anomalously weak SH feedback and vice versa. This explains why the spread of global-mean long-term LR+WV feedback is considerably smaller than that of interannual counterpart, and why the spread of tropical-mean long-term LR+WV feedback is twice as large as that of global-mean feedback.

Following Held and Shell (2012), we further decompose the LR+WV feedback into WV feedback caused by the vertical-uniform warming under fixed relative humidity (fixed-RH) condition ($WV_{uniform}$ feedback), LR feedback under fixed-RH condition (or the sum of LR feedback and its corresponding WV feedback component under fixed-RH condition; $\widetilde{LR}$ feedback) and relative humidity (RH) feedback, as following:

$$LR + WV = WV_{uniform} + \widetilde{LR} + RH$$

The contribution of local uncertainty to the spread of global-mean LR+WV feedbacks are shown for each component (Figure 3c-h). The decomposition reveals that the large uncertainties in LR+WV feedback over the tropics comes from intermodel uncertainties in RH feedback (Figure 3a-b & 3g-h). In other words, the spread of global-mean LR+WV feedback is dominated by differences in the tropical RH feedback, with a correlation [0.94 (0.98)] between long-term, global-mean (tropical-mean) LR+WV and RH feedbacks (Figure 1c & S1b). For the same reasons, the RH feedback also cannot be constrained with observations (Figure 1d & S1c).

The local, offsetting extratropical contributions to the global-mean long-term LR+WV feedback spread mostly come from local uncertainties of $WV_{uniform}$ feedback (Figure 3a-d). The hemispheric asymmetry of $WV_{uniform}$ uncertainty contribution pattern also partly reflects the meridional warming asymmetry. Meanwhile, signals are weak in the uncertainty contribution pattern of $\widetilde{LR}$ feedback (Figure 3e-f). Similar patterns of local contribution occur under all-sky conditions (Figure S3c-h), although the contribution magnitude is larger in some cases. For instance, there are larger positive contributions from local uncertainties of all-sky $\widetilde{LR}$ feedback over the NH (Figure S3e-f), compared to those under clear-sky conditions (Figure 3c-f). These are primarily due to the above-mentioned differences in cloud climatologies, especially the representation of cloud top height. The differences in local contribution from clear-sky and all-sky $\widetilde{LR}$ feedback spread suggest a much larger uncertainty of the simulated cloud top height occurs over the northern extratropics (NE) than the southern extratropics (SE).

Our findings differ from the CMIP5 analyses by Po-Chedley et al. (2018) in a few ways. First, they showed that model differences in all-sky $\widetilde{LR}$ feedback over the SE drive the model variability in global-mean long-term all-sky LR+WV feedback. We find the contribution of $\widetilde{LR}$ feedback to the global-mean LR+WV feedback concentrated in the NH for all-sky condition (Figure S3e-f), and small overall. Instead, the uncertainty in LR+WV feedback mostly comes from the tropics, where local RH exhibits the largest intermodel disagreement, especially under clear-sky condition (Figure 3a-b & 3g-h). Additionally, their reported high correlation (r = 0.99) between all-sky LR+WV and $\widetilde{LR}$ feedbacks decreases by one-fourth in our analyses (Figure S1d). This discrepancy could be attributed to more consistent cloud climatologies over the SE in CMIP6-era models (Vignesh et al., 2020). However, it should be noted that the local feedback calculation is different, as their calculations use local surface air temperature anomalies instead of global-mean surface air temperature anomalies and thus are more strongly influenced by local warming asymmetries.

The question then arises: Do differences in warming patterns modify these climate feedbacks? To answer this question, we extend our analysis to uncertainties in local surface air temperature changes, by cross-model regressing the last 20-years local surface air temperature change to quadrupling CO_2 against the global-mean long-term feedbacks (Figure 4). In terms of the spread in long-term cloud feedback, positive contribution from local warming uncertainty is evident almost everywhere (Figure 4a). This roughly uniform positive contribution can be interpreted by the fixed anvil temperature for high cloud feedback (Figure S2f; Hartmann & Larson, 2002; Zelinka & Hartmann, 2010) and low cloud thermodynamic and stability mechanisms for shortwave cloud feedback (Figure 2d & S2d; Klein & Hartmann, 1993; Wood & Bretherton, 2006; Bretherton, 2015; Qu et al., 2015). The distinct west-east contrast over the tropical Pacific has been noted in previous studies (Ceppi & Gregory, 2017; Andrews & Webb, 2018) and shown to modulate cloud feedback over the tropical eastern Pacific, further influencing the spread of global-mean cloud feedback. The high uncertainty contribution over polar regions is likely due to the high correlation between global-mean warming and polar amplification. In contrast, the spread of long-term LR+WV feedbacks is driven by a meridional asymmetry (Figure 4b & S4). This is consistent with the above-mentioned uncertainty contribution pattern of $WV_{uniform}$ feedback. The most noticeable contribution occurs over the Southern Ocean (Figure 4b), where uncertainty in ocean heat uptake plays an essential role in manipulating the regional warming extent. This is consistent with Po-Chedley et al. (2018). Under all-sky conditions, however, the local warming contribution occurs in the NE instead of the SE. This supports our previous interpretation that a larger intermodel difference in cloud climatologies occurs over the NE than the SE. To some extent, this can be attributed to the more accurate representation of supercooled liquid cloud water over the SE in CMIP6-era models (Zelinka et al. 2020).

4. Conclusions and discussion

Here observation-based emergent constraints are adopted to evaluate the intermodel spread in long-term cloud and LR+WV feedbacks. The results indicate that observed interannual variation provides a useful constraint to narrow the uncertainty in global-mean long-term cloud feedback. Similar regional uncertainty contributions on both interannual and long-term timescales reflect a consistent behavior of low cloud changes and bolster the effectiveness of the observed constraint. Additionally, the local contribution to the long-term cloud feedback spread is dominated by the shortwave, low cloud feedback.

In contrast, the long-term LR+WV feedback cannot be constrained with observations of interannual variability. This arises for two reasons: i) the spread of global-mean long-term LR+WV feedback is only half as large as that of interannual feedback; and ii) the observed uncertainty from individual observation nearly equals to the intermodel spread of global-mean interannual LR+WV feedback. Additionally, there is a large discrepancy among different observations and reanalyses products on the value of interannual LR+WV feedback. The spread of global-mean long-term LR+WV feedback is dominated by the tropics, where the largest contribution comes from the uncertainties in local relative humidity (RH) feedback, with a remarkably high correlation between LR+WV and RH feedbacks. Local intermodel uncertainties over the northern and southern extratropics, which are associated with the WV feedback under vertical-uniform warming and fixed-RH condition, offset each other. As a result, the uncertainty of tropical-mean LR+WV feedback is twice as large as that of global-mean feedback. Model differences in hemispheric warming asymmetries, induced primarily by Southern Ocean (SO) heat uptake differences, provide a secondary contribution to the spread in long-term LR+WV feedback.

The importance of uncertainty in RH feedback is highlighted in this work. However, what causes the intermodel uncertainty still remains unknown. Here, some potential causes are proposed. First, the tropical RH feedback uncertainty could be related to the diversity of convective schemes adopted by CMIP6 models. For example, differences in the convective adjustment to exceeded saturation and the autoconversion from cloud water to rain in convective systems can greatly influence RH distributions (e.g., Zhao, 2014; Zhao et al., 2016). Second, the asymmetric contribution pattern of RH feedback over the tropics on long-term timescales could also be attributed to the difference in Intertropical Convergence Zone (ITCZ) shift to anthropogenic forcing (Byrne et al., 2018), which is closely tied to the meridional warming asymmetry. Related, the asymmetric contribution pattern could also result from inherited double-ITCZ bias, since the negative contribution occurs over the southeastern Pacific and South Atlantic, where a fictitious ITCZ is simulated by vast majority of climate models. In this case, models with less (more) double-ITCZ bias would be less (more) affected by the narrowed ITCZ under anthropogenic forcing and thereby a larger (smaller) RH feedback. These hypotheses add to the growing list of documented relationships between ECS and double-ITCZ bias in models (Tian, 2015; Webb and Lock, 2020). Third, given the close relation between convective aggregation strength and double-peak structure of tropical rainbelt (Popp and Bony, 2019) and the high negative correlation between convective aggregation and RH feedback (Bony et al., 2020) in observations, it is reasonable to suspect a physical causality between convective aggregation strength and RH feedback. Models with stronger convective aggregation would have larger double-ITCZ biases and therefore have smaller RH feedbacks. A detailed investigation of the causes of RH feedback uncertainty remains the subject of future work.

While the pattern of local warming contribution to the global-mean long-term LR+WV feedback suggests the SO heat uptake plays a role, a direct connection is not immediately obvious. For example, less warming due to more SO heat uptake should lead to a smaller local LR+WV feedback, not the larger global-mean LR+WV feedback as we find. Hence, the SO heat uptake likely exerts its impact on the global-mean LR+WV feedback in indirect ways, for instance by suppressing ocean heat uptake and leveraging a larger fraction of surface warming over the northern extratropics via a weakened Atlantic meridional overturning circulation. Alternatively, the SO heat uptake may modulate the global-mean LR+WV feedback by amplifying the meridional warming asymmetry, which could lead to the ITCZ shift, thereby modifying the LR+WV feedback. In this case, our results could explain a common feature that models with the more ocean heat uptake are the models with the higher ECS (Armour, 2017), since models with the more ocean heat uptake would also have a larger global-mean long-term LR+WV feedback.

Acknowledgments

HH and BJS are supported by NASA award 80NSSC18K1032. RJK is supported by an appointment to the NASA Postdoctoral Program administered by Universities Space Research Association.

Competing Interests

Authors have no competing interests.

Data Availability Statement

The CMIP6 data are available at https://esgf-node.llnl.gov/search/cmip6/. The CERES radiative flux observations are available at https://ceres.larc.nasa.gov/data/. The GISTEMP is available at https://data.giss.nasa.gov/gistemp/. The ERA5 reanalysis data are available at https://cds.climate.copernicus.eu/#!/search?text=ERA5&type=dataset. The AIRS temperature and water vapor observations and the MERRA-2 reanalysis data are available at https://disc.gsfc.nasa.gov/. The CloudSat/CALIPSO radiative kernels used in this study and related code for applying them are available at https://climate.rsmas.miami.edu/data/radiative-kernels/.

Reference

Andrews, T., & Webb, M. J. (2018). The dependence of global cloud and lapse rate feedbacks on the spatial structure of tropical Pacific warming. Journal of Climate, 31(2), 641 – 654. https://doi.org/10.1175/JCLI-D-17-0087.1

Aumann, H. H., & Coauthors, (2003). AIRS/AMSU/HSB on the Aqua mission: Design, science objectives, data products, and processing systems. IEEE Transactions on Geoscience and Remote Sensing, 41, 253–264. doi: 10.1109/TGRS.2002.808356.

Armour, K. C. (2017). Energy budget constraints on climate sensitivity in light of inconstant climate feedbacks. Nature Climate Change, 7(5), 331–335. https://doi.org/10.1038/nclimate3278

Bjordal, J., Storelvmo, T., Alterskjær, K., & Carlsen, T. (2020). Equilibrium climate sensitivity above 5 °C plausible due to state-dependent cloud feedback. Nature Geoscience, 13, 718–721. https://doi.org/10.1038/s41561-020-00649-1

Bony, S., & Coauthors, (2006). How well do we understand and evaluate climate change feedback processes? Journal of Climate, 19, 3445–3482, https://doi.org/10.1175/JCLI3819.1.

Bony, S., Semie, A., Kramer, R. J., Soden, B., Tompkins, A. M., & Emanuel, K. A. (2020). Observed modulation of the tropical radiation budget by deep convective organization and lower-tropospheric stability. AGU Advances, 1, e2019AV000155. https://doi.org/10.1029/2019AV000155

Bretherton, C. S. (2015). Insights into low-latitude cloud feed- backs from high-resolution models. Philosophical Transactions of the Royal Society A: Mathematical, Physical and Engineering Sciences, 373, 3354–3360. http://doi.org/10.1098/rsta.2014.0415

Byrne, M. P., Pendergrass, A. G., Rapp, A. D., & Wodzicki, K. R. (2018). Response of the intertropical convergence zone to climate change: Location, width, and strength. Current Climate Change Reports, 4(4), 355–370. https://doi.org/10.1007/s40641-018-0110-5

Ceppi, P., & Gregory, J. M. (2017). Relationship of tropospheric stability to climate sensitivity and Earth's observed radiation budget. Proceedings of the National Academy of Sciences of the United States of America, 114(50), 13,126–13,131. https://doi.org/10.1073/pnas.1714308114

Chung, E. S., Yeomans, D., & Soden, B. J. (2010). An assessment of climate feedback processes using satellite observations of clear-sky OLR. Geophysical Research Letters, 37, L02702, https://doi:10.1029/2009GL041889

Chung, E.-S., & Soden, B. J. (2015). An assessment of direct radiative forcing, radiative adjustments, and radiative feedbacks in coupled ocean–atmosphere models. Journal of Climate, 28(10), 4152–4170. https://doi.org/10.1175/JCLI-D-14-00436.1

Colman, R. (2003). A comparison of climate feedbacks in GCMs. Climate Dynamics, 20, 865–873. https://doi.org/10.1007/s00382-003-0310-z

Dessler, A. E. (2013). Observations of climate feedbacks over 2000–2010 and comparisons to climate models. Journal of Climate, 26, 333–342, doi:10.1175/JCLI-D-11-00640.1

Dufresne, J.-L. & Bony, S. (2008). An assessment of the primary sources of spread of global warming estimates from coupled atmosphere–ocean models. Journal of Climate, 21, 5135–5144, https://doi.org/10.1175/2008JCLI2239.1

Eyring, V., Bony, S., Meehl, G. A., Senior, C. A., Stevens, B., Stouffer, R. J., & Taylor, K. E. (2016). Overview of the Coupled Model Intercomparison Project Phase 6 (CMIP6) experimental design and organization. Geoscientific Model Development, 9(5), 1937–1958, https://doi:10.5194/gmd-9-1937-2016

Flato, G., & Coauthors, (2013). Evaluation of climate models. In Stocker, T. F., Qin, D., Plattner, G.-K., Tignor, M., Allen, S.K., Boschung, J., Nauels, A., Xia, Y., Bex, V., & Midgley P. M. (eds.), Climate Change 2013: The Physical Science Basis. Contribution of Working Group I to the Fifth Assessment Report of the Intergovernmental Panel on Climate Change (pp. 741–882). Cambridge, United Kingdom and New York, NY, USA: Cambridge University Press.

Gelaro, R., & Coauthors, (2017). The Modern‐Era Retrospective Analysis for Research and Applications, Version 2 (MERRA ‐ 2). Journal of Climate, 30(14), 5419 – 5454. https://doi.org/10.1175/JCLI-D-16-0758.1

GISTEMP‐Team (2019). GISS Surface Temperature Analysis (GISTEMP), version 4. NASA Goddard Institute for Space Studies. Dataset accessed 2016 ‐ 09 ‐ 27 at https://data.giss.nasa.gov/gistemp/

Hall, A., & Qu, X. (2006). Using the current seasonal cycle to constrain snow albedo feedback in future climate change. Geophysical Research Letters, 33:L03502. https://doi:10.1029/2005GL025127

Hartmann, D. L., & Larson, K. (2002). An important constraint on tropical cloud–climate feedback. Geophysical Research Letters, 29:1951. doi:10.1029/2002GL015835

Held, I. M., & Shell, K. M. (2012). Using relative humidity as a state variable in climate feedback analysis. Journal of Climate, 25(8), 2578–2582. https://doi.org/10.1175/JCLI-D-11-00721.1

Hofmann, D. J., Butler, J. H., Dlugokencky, E. J., Elkins, J. W., Masarie, K., Montzka, S. A., & Tans, P. (2006). The role of carbon dioxide in climate forcing from 1979–2004: Introduction of the Annual Greenhouse Gas Index. Tellus, 58B, 614–619. https://doi.org/10.1111/j.1600-0889.2006.00201.x

Klein, S. A., & Hartmann, D. L. (1993). The seasonal cycle of low stratiform clouds. Journal of Climate, 6:1587–1606. https://doi.org/10.1175/1520-0442(1993)006<1587:TSCOLS>2.0.CO;2

Klein, S. A., & Hall, A. (2015). Emergent constraints for cloud feedbacks. Current Climate Change Reports, 1, 276–287. https://doi.org/10.1007/s40641-015-0027-1

Kramer, R. J., Matus, A. V., Soden, B. J., & L'Ecuyer, T. S. (2019). Observation-based radiative kernels from CloudSat/CALIPSO. Journal of Geophysical Research: Atmospheres, 124, 5431–5444. https://doi.org/10.1029/2018JD029021

Kramer, R. J., He, H., Soden, B. J., Oreopoulos, L., Myhre, G., Forster, P. M., & Smith, C. J. (2021) Observational evidence of increasing global radiative forcing. Submitted to Geophysical Research Letters

Lenssen, N., G. Schmidt, J. Hansen, M. Menne, A. Persin, R. Ruedy, and D. Zyss, (2019). Improvements in the GISTEMP uncertainty model. Journal of Geophysical Research: Atmospheres, 124, 6307– 6326. https://doi.org/10.1029/2018JD029522

Loeb, N. G., Doelling, D. R., Wang, H., Su, W., Nguyen, C., Corbett, J. G., Liang, L., Mitrescu, C., Rose, F. G., & Kato, S. (2018). Clouds and the Earth's Radiant Energy System (CERES) Energy Balanced and Filled (EBAF) Top-of-Atmosphere (TOA) Edition-4.0 Data Product. Journal of Climate, 31(2), 895–918. https://doi.org/10.1175/JCLI-D-17-0208.1

Loeb, N. G., Rose, F. G., Kato, S., Rutan, D. A., Su, W., Wang, H., Doelling, D. R., Smith, W. L., & Gettelman, A. (2019). Towards a consistent definition between satellite and model clear-sky radiative fluxes. Journal of Climate, 33, 61–75. https://doi.org/10.1175/jcli-d-19-0381.1

Montzka, S. A., Dlugokencky, E. J. & Butler, J. H. (2011). Non-CO2 greenhouse gases and climate change. Nature, 476, 43–50. https://doi.org/10.1038/nature10322

Po-Chedley, S., Armour, K. C., Bitz, C. M., Zelinka, M. D., & Santer, B. D. (2018). Sources of intermodel spread in the lapse rate and water vapor feedbacks. Journal of Climate, 31(8), 3187–3206. https://doi.org/10.1175/JCLI-D-17-0674.1

Popp, M., & Bony, S. (2019). Stronger zonal convective clustering associated with a wider tropical rain belt. Nature Communications, 10(1), 4261. https://doi.org/10.1038/s41467-019-12167-9

Qu, X., & Hall, A. (2014). On the persistent spread in snow-albedo feedback. Climate Dynamics, 42(1), 69–81, https://doi:10.1007/s00382-013-1774-0

Qu, X., Hall, A., Klein, S. A., & Caldwell, P. M. (2015). The strength of the tropical inversion and its response to climate change in 18 CMIP5 models. Climate Dynamics, 45, 375–396. https://doi.org/10.1007/s00382-014-2441-9

Santer, B. D., Wigley, T. M. L., Mears, C., Wentz, F. J., Klein, S. A., Seidel, D. J., et al. (2005). Amplification of surface temperature trends and variability in the tropical atmosphere. Science (New York, N.Y.), 309(5740), 1551–1556. DOI: 10.1126/science.1114867

Sherwood, S. C., & Coauthors, (2020). An assessment of Earth's climate sensitivity using multiple lines of evidence. Reviews of Geophysics, 58, e2019RG000678. https://doi.org/10.1029/2019RG000678

Soden, B. J., & Held, I. M. (2006). An assessment of climate feed- backs in coupled ocean–atmosphere models. Journal of Climate, 19, 3354–3360. https://doi.org/10.1175/JCLI3799.1

Soden, B. J., Held, I. M., Colman, R., Shell, K. M., Kiehl, J. T., & Shields, C. A. (2008). Quantifying climate feedbacks using radiative kernels. Journal Climate, 21, 3504–3520. https://doi.org/10.1175/2007JCLI2110.1

Soden, B. J., & Vecchi, G. A. (2011). The vertical distribution of cloud feedback in coupled ocean-atmosphere models. Geophysical Research Letters, 38, L12704. https://doi.org/10.1029/2011GL047632

Tian, B. (2015). Spread of model climate sensitivity linked to double-Intertropical Convergence Zone bias. Geophysical Research Letters, 42,4133–4141. https://doi.org/10.1002/2015GL064119

Vignesh, P. P., Jiang, J. H., Kishore, P., Su, H., Smay, T., Brighton, N., & Velicogna, I. (2020). Assessment of CMIP6 cloud fraction and comparison with satellite observations. Earth and Space Science, 7, e2019EA000975. https://doi.org/10.1029/2019EA000975

Webb, M. J., Senior, C. A., Sexton, D. M. H., Ingram, W. J., Williams, K. D., Ringer, M. A., & Taylor, K. E. (2006). On the contribution of local feedback mechanisms to the range of climate sensitivity in two GCM ensembles. Climate Dynamics, 27, 17–38. https://doi.org/10.1007/s00382-006-0111-2

Webb, M. J., & Lock, A. P. (2020). Testing a physical hypothesis for the relationship between climate sensitivity and double-ITCZ bias in climate models. Journal of Advances in Modeling Earth Systems, 12, e2019MS001999. https://doi.org/10.1029/2019MS001999

Wood, R., & Bretherton, C. S. (2006). On the relationship between stratiform low cloud cover and lower-tropospheric stability. Journal of Climate, 19:6425–6432. https://doi.org/10.1175/JCLI3988.1

Zelinka, M. D., & Hartmann, D. L. (2010). Why is longwave cloud feedback positive? Journal of Geophysical Research: Atmospheres, 115:D16117. doi:10.1029/2010JD013817.

Zelinka, M. D., Myers, T. A., McCoy, D. T., Po-Chedley, S., Caldwell, P. M., Ceppi, P., Klein, S. A., & Taylor, K. E. (2020). Causes of higher climate sensitivity in CMIP6 models. Geophysical Research Letters, 47, e2019GL085782. https://doi.org/10.1029/2019GL085782

Zhao, M. (2014). An investigation of the connections among convection, clouds, and climate sensitivity in a global climate model. Journal of Climate, 27:1845–1862. https://doi.org/10.1175/JCLI-D-13-00145.1

Zhao, M., & Coauthors, (2016). Uncertainty in model climate sensitivity traced to representations of cumulus precipitation microphysics. Journal of Climate, 29:543–560. https://doi.org/10.1175/JCLI-D-15-0191.1

Zhou, C., Zelinka, M. D., Dessler, A. E., & Klein, S. A. (2015). The relationship between interannual and long-term cloud feedbacks. Geophysical Research Letters, 42, 10,463–10,469, https://doi:10.1002/2015GL066698

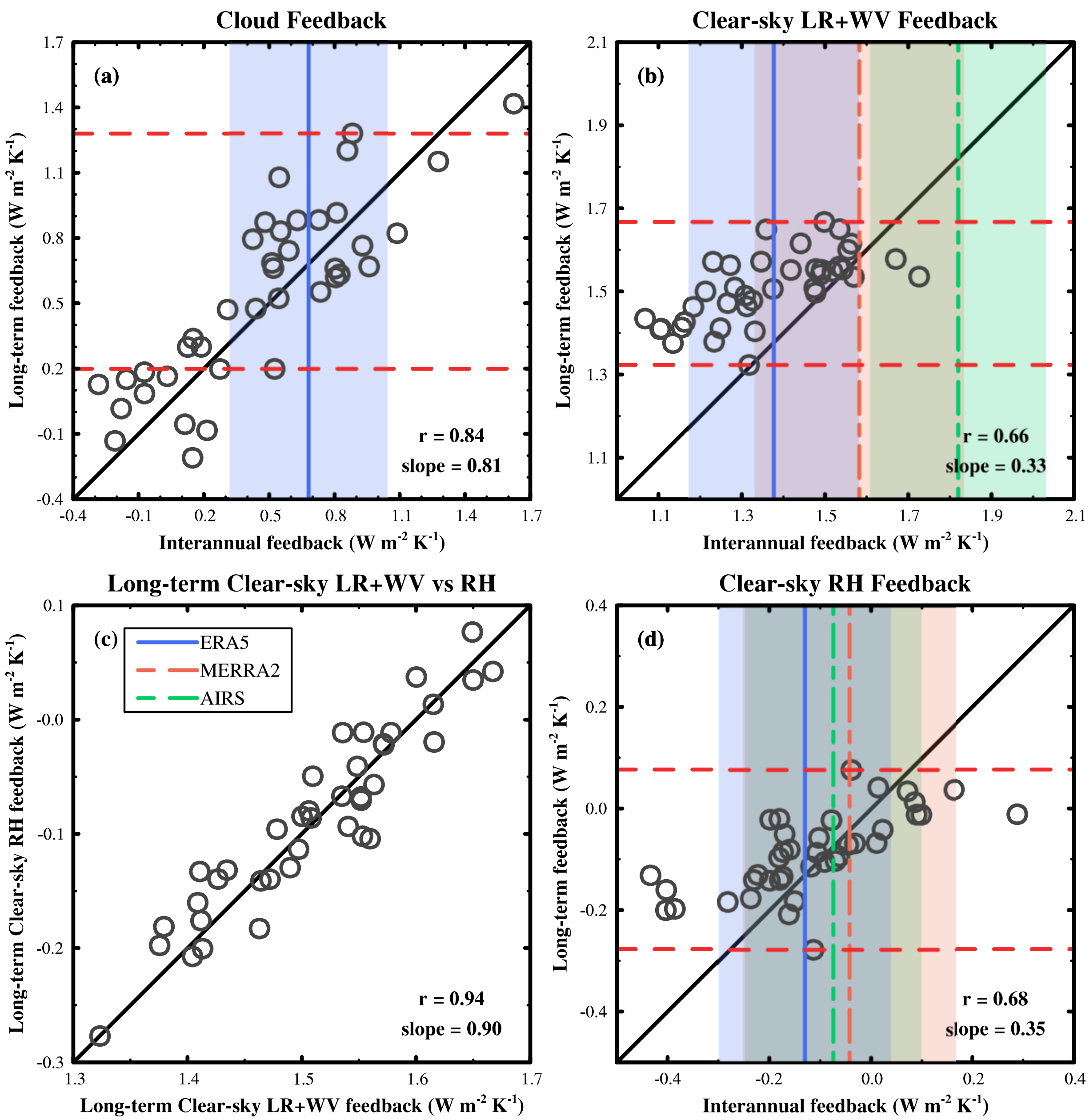

Figure 1. Scatterplots of global-mean interannual (a) cloud feedback, (b) LR+WV feedback and (d) relative humidity feedback versus their corresponding long-term feedbacks and (c) a comparison between long-term LR+WV and relative humidity feedbacks in 39 CMIP6 models. The lines denote observed interannual feedbacks, while the shadings show their corresponding 95% confidence intervals. The red horizonal dash lines highlighted the spreads of long-term feedbacks are based on observed emergent constraints using ERA5 vertical temperature and humidity profiles.

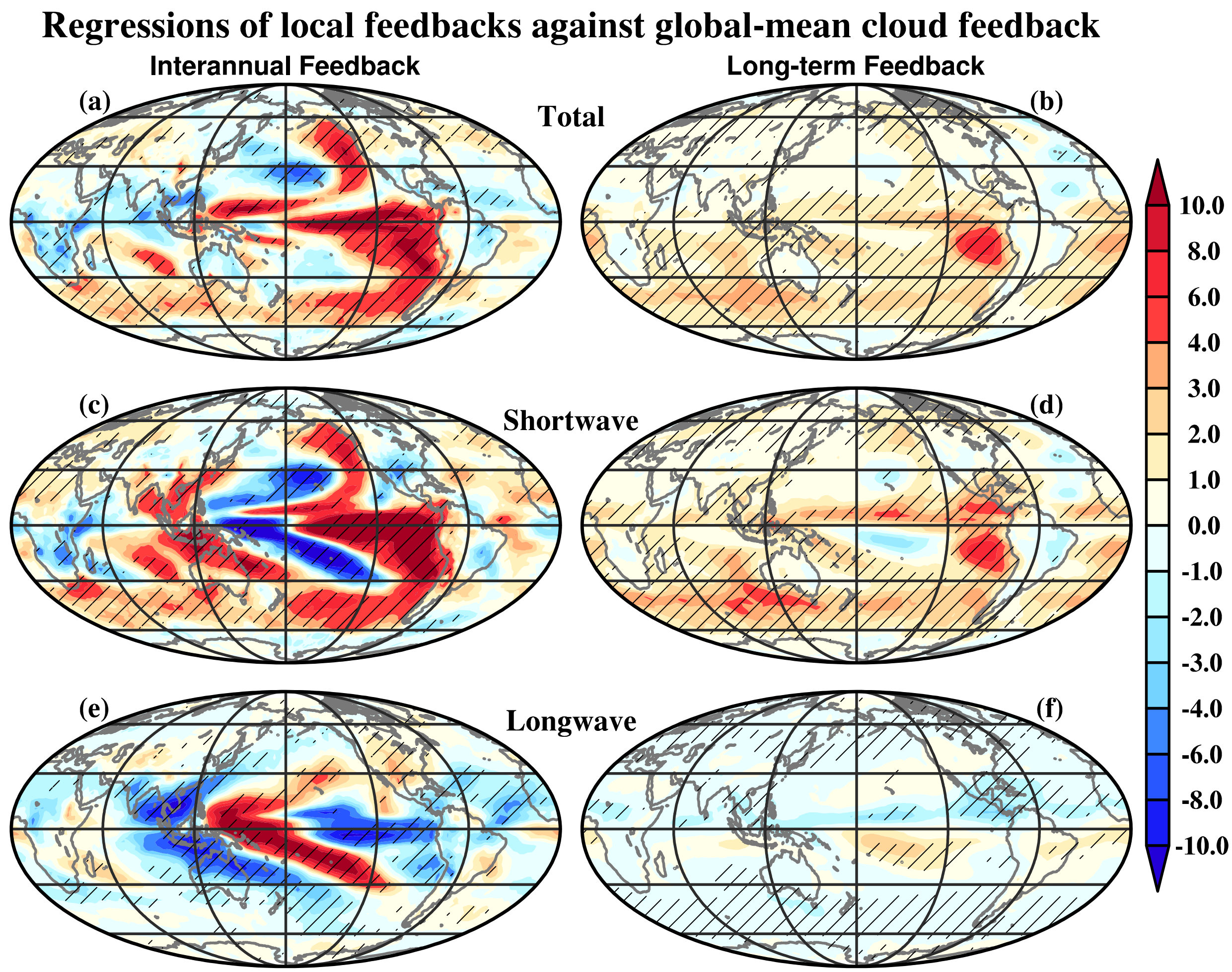

Figure 2. Cross-model regressions of local (a-b) cloud feedback, (c-d) shortwave cloud feedback and (e-f) longwave cloud feedback against global-mean cloud feedback for both (a, c and e) interannual and (b, d and f) long-term timescales. Hatching indicates area where regression is statistically significant at the 95% level.

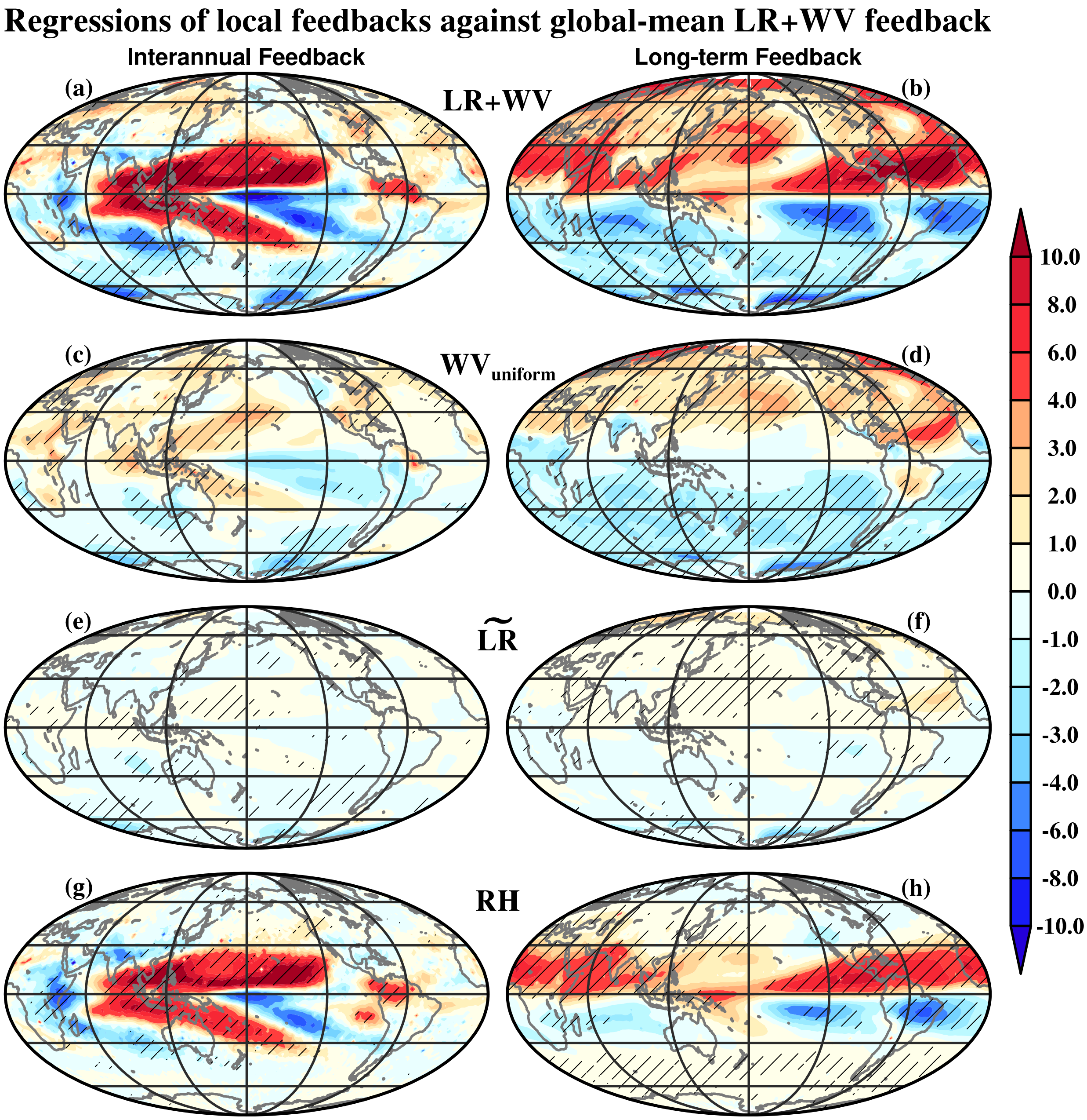

Figure 3. Cross-model regressions of local (a-b) LR+WV feedback, (c-d) $WV_{uniform}$ feedback, (e-f) $\widetilde{LR}$ feedback and (g-h) RH feedback against global-mean LR+WV feedback for both (a, c, e and g) interannual and (b, d, f and h) long-term timescales. Hatching indicates area where regression is statistically significant at the 95% level.

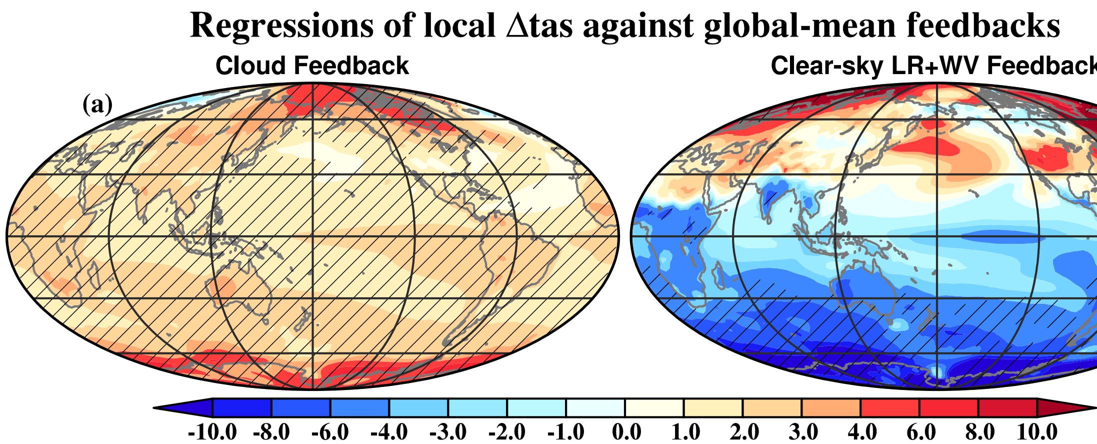

Figure 4. Cross-model regressions of last 20-years local surface air temperature change of abrupt-4xCO2 runs to global-mean long-term (a) cloud feedback and (b) LR+WV feedback. Hatching indicates area where regression is statistically significant at the 95% level.

Supplementary Materials for

Constraining the Intermodel Spread in Cloud and Water Vapor Feedback

Haozhe He[1], Ryan J. Kramer[2,3], Brian J. Soden[1]

[1]Rosenstiel School of Marine and Atmospheric Science, University of Miami, Miami, FL, USA

[2]Climate and Radiation Laboratory, NASA Goddard Space Flight Center, Greenbelt, MD, USA

[3]Universities Space Research Association, Columbia, MD, USA

Correspondence to: Haozhe He, haozhe.he@rsmas.miami.edu

Submitted to Geophysical Research Letters

Table S1. A list of the CMIP6 climate models analyzed in this study.

	Institution	**Model**	**DOI piControl**	**DOI abrupt-4xCO2**
1	CSIRO-ARCCSS	ACCESS-CM2	doi:10.22033/ESGF/CMIP6.4311	doi:10.22033/ESGF/CMIP6.4237
2	CSIRO	ACCESS-ESM1-5	doi:10.22033/ESGF/CMIP6.4312	doi:10.22033/ESGF/CMIP6.4238
3	AWI	AWI-CM-1-1-MR	doi:10.22033/ESGF/CMIP6.2777	doi:10.22033/ESGF/CMIP6.2568
4	BCC	BCC-CSM2-MR	doi:10.22033/ESGF/CMIP6.3016	doi:10.22033/ESGF/CMIP6.2845
5	BCC	BCC-ESM1	doi:10.22033/ESGF/CMIP6.3017	doi:10.22033/ESGF/CMIP6.2846
6	CAMS	CAMS-CSM1-0	doi:10.22033/ESGF/CMIP6.9797	doi:10.22033/ESGF/CMIP6.9708
7	CCCma	CanESM5	doi:10.22033/ESGF/CMIP6.3673	doi:10.22033/ESGF/CMIP6.3532
8	NCAR	CESM2	doi:10.22033/ESGF/CMIP6.7733	doi:10.22033/ESGF/CMIP6.7519
9	NCAR	CESM2-FV2	doi:10.22033/ESGF/CMIP6.11301	doi:10.22033/ESGF/CMIP6.11285
10	NCAR	CESM2-WACCM	doi:10.22033/ESGF/CMIP6.10094	doi:10.22033/ESGF/CMIP6.10039
11	NCAR	CESM2-WACCM-FV2	doi:10.22033/ESGF/CMIP6.11302	doi:10.22033/ESGF/CMIP6.11286
12	THU	CIESM	doi:10.22033/ESGF/CMIP6.8849	doi:10.22033/ESGF/CMIP6.8807
13	CMCC	CMCC-CM2-SR5	doi:10.22033/ESGF/CMIP6.3874	doi:10.22033/ESGF/CMIP6.3731
14	DOE	E3SM-1-0	doi:10.22033/ESGF/CMIP6.4499	doi:10.22033/ESGF/CMIP6.4491
15	EC-Earth-Consortium	EC-Earth3-AerChem	doi:10.22033/ESGF/CMIP6.4843	doi:10.22033/ESGF/CMIP6.4519
16	EC-Earth-Consortium	EC-Earth3-Veg	doi:10.22033/ESGF/CMIP6.4848	doi:10.22033/ESGF/CMIP6.4524
17	CAS	FGOALS-f3-L	doi:10.22033/ESGF/CMIP6.3447	doi:10.22033/ESGF/CMIP6.3176
18	CAS	FGOALS-g3	doi:10.22033/ESGF/CMIP6.3448	doi:10.22033/ESGF/CMIP6.3177
19	NOAA-GFDL	GFDL-CM4	doi:10.22033/ESGF/CMIP6.8666	doi:10.22033/ESGF/CMIP6.8486
20	NOAA-GFDL	GFDL-ESM4	doi:10.22033/ESGF/CMIP6.8669	doi:10.22033/ESGF/CMIP6.8489
21	NASA-GISS	GISS-E2-1-G	doi:10.22033/ESGF/CMIP6.7380	doi:10.22033/ESGF/CMIP6.6976
22	NASA-GISS	GISS-E2-1-H	doi:10.22033/ESGF/CMIP6.7381	doi:10.22033/ESGF/CMIP6.6977
23	NASA-GISS	GISS-E2-2-G	doi:10.22033/ESGF/CMIP6.7382	doi:10.22033/ESGF/CMIP6.6978
24	CCCR-IITM	IITM-ESM	doi:10.22033/ESGF/CMIP6.3710	doi:10.22033/ESGF/CMIP6.3516
25	INM	INM-CM4-8	doi:10.22033/ESGF/CMIP6.5080	doi:10.22033/ESGF/CMIP6.4931
26	INM	INM-CM5-0	doi:10.22033/ESGF/CMIP6.5081	doi:10.22033/ESGF/CMIP6.4932
27	IPSL	IPSL-CM6A-LR	doi:10.22033/ESGF/CMIP6.5251	doi:10.22033/ESGF/CMIP6.5109
28	NIMS-KMA	KACE-1-0-G	doi:10.22033/ESGF/CMIP6.8425	doi:10.22033/ESGF/CMIP6.8348
29	KIOST	KIOST-ESM	doi:10.22033/ESGF/CMIP6.5303	doi:10.22033/ESGF/CMIP6.5288
30	MIROC	MIROC6	doi:10.22033/ESGF/CMIP6.5711	doi:10.22033/ESGF/CMIP6.5411
31	HAMMOZ-Consortium	MPI-ESM-1-2-HAM	doi:10.22033/ESGF/CMIP6.5037	doi:10.22033/ESGF/CMIP6.5000
32	MPI-M	MPI-ESM1-2-HR	doi:10.22033/ESGF/CMIP6.6674	doi:10.22033/ESGF/CMIP6.6458
33	MPI-M	MPI-ESM1-2-LR	doi:10.22033/ESGF/CMIP6.6675	doi:10.22033/ESGF/CMIP6.6459
34	MRI	MRI-ESM2-0	doi:10.22033/ESGF/CMIP6.6900	doi:10.22033/ESGF/CMIP6.6755
35	NUIST	NESM3	doi:10.22033/ESGF/CMIP6.8776	doi:10.22033/ESGF/CMIP6.8719
36	NCC	NorESM2-LM	doi:10.22033/ESGF/CMIP6.8217	doi:10.22033/ESGF/CMIP6.7836
37	NCC	NorESM2-MM	doi:10.22033/ESGF/CMIP6.8221	doi:10.22033/ESGF/CMIP6.7840
38	SNU	SAM0-UNICON	doi:10.22033/ESGF/CMIP6.7791	doi:10.22033/ESGF/CMIP6.7783
39	AS-RCEC	TaiESM1	doi:10.22033/ESGF/CMIP6.9798	doi:10.22033/ESGF/CMIP6.9709

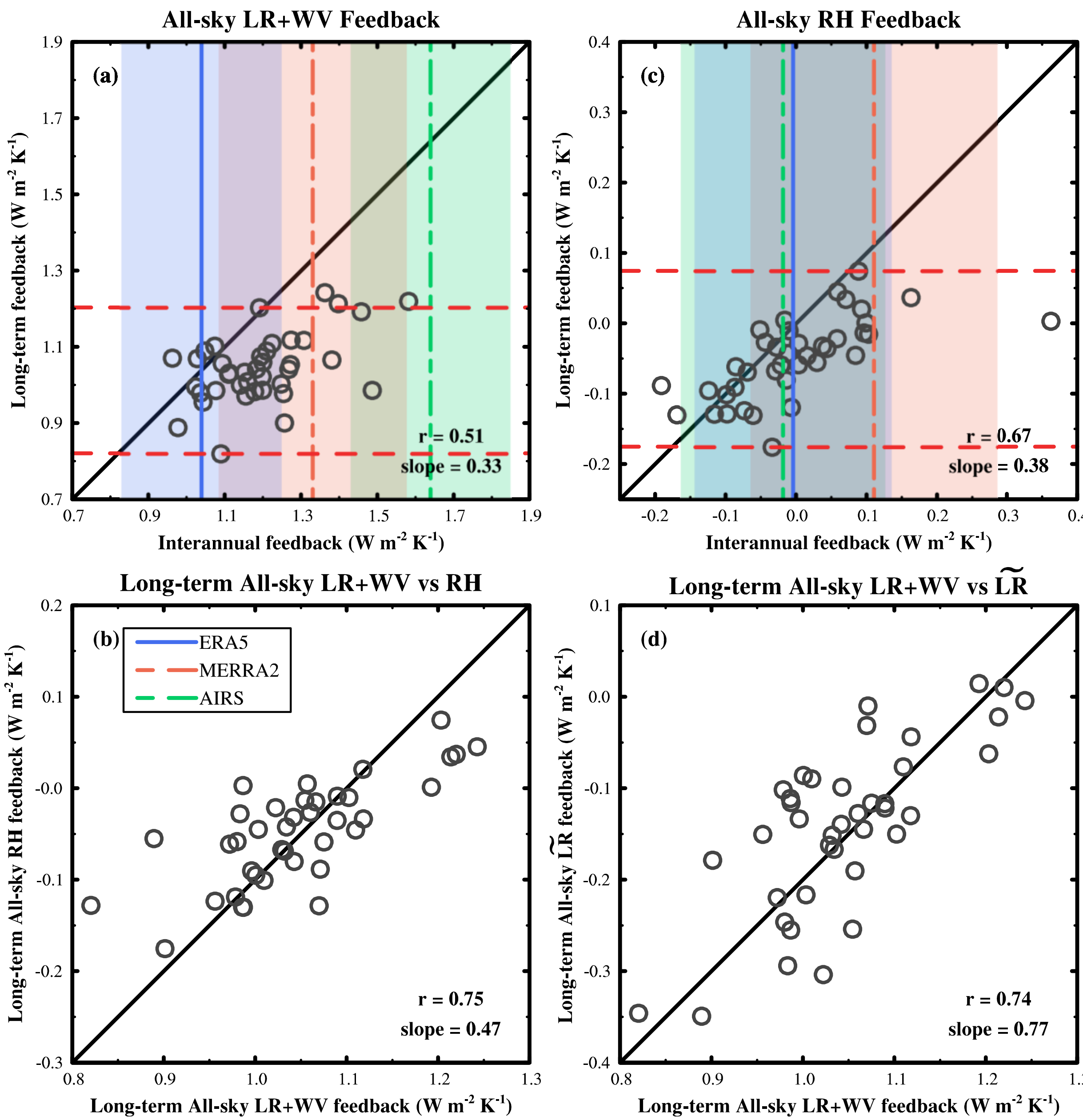

Figure S1. (a-c) are same as Figure 1b, 1c and 1d, except for all-sky condition and (d) a comparison between long-term all-sky LR+WV and relative humidity fixed lapse-rate feedbacks in 39 CMIP6 models.

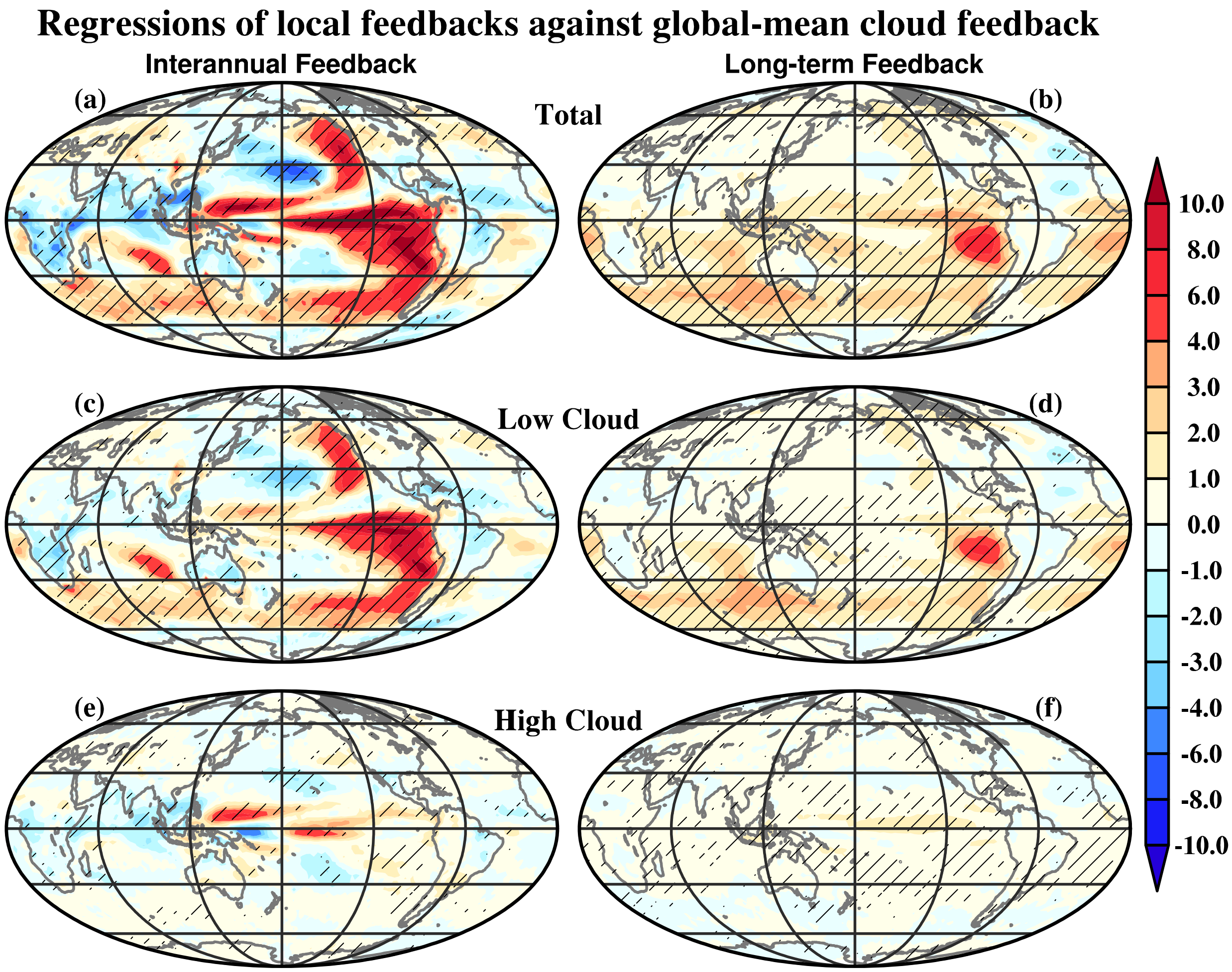

Figure S2. Cross-model regressions of local (a-b) cloud feedback, (c-d) low cloud feedback and (e-f) high cloud feedback against global-mean cloud feedback for both (a, c and e) interannual and (b, d and f) long-term timescales. Hatching indicates area where regression is statistically significant at the 95% level.

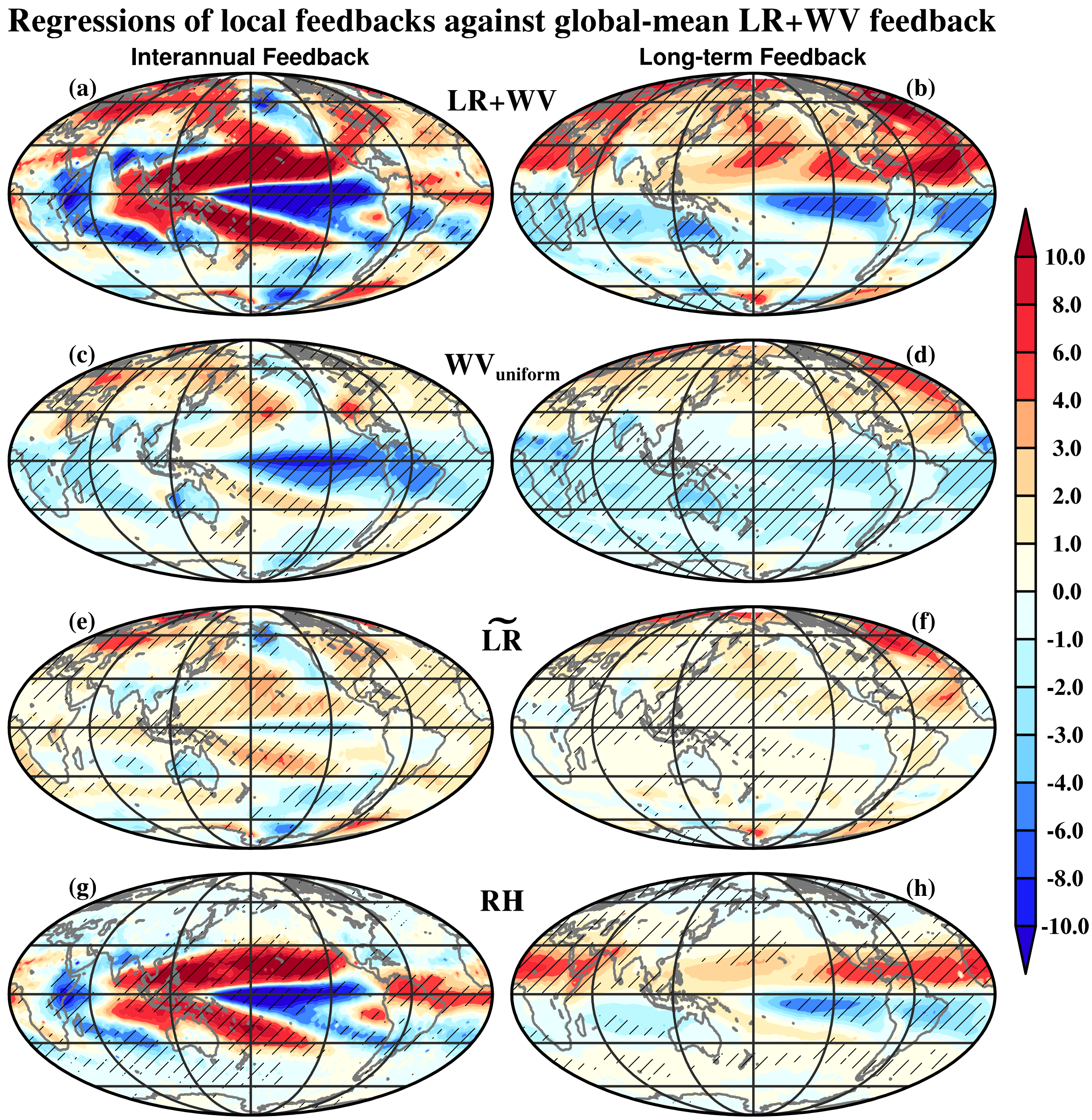

Figure S3. Same as Figure 3, except for all-sky condition.

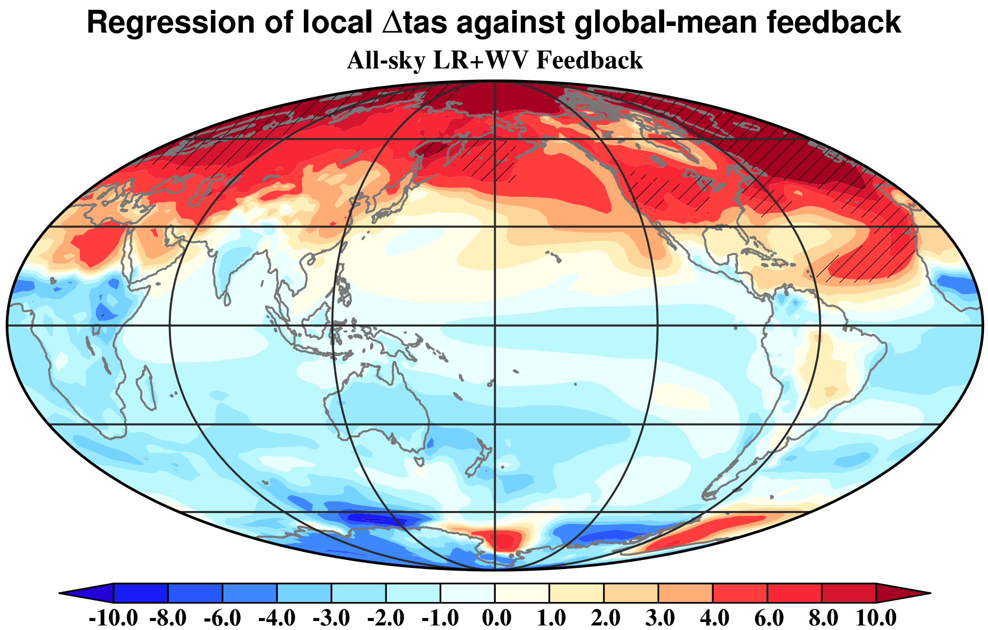

Figure S4. Same as Figure 4b, except for all-sky condition.